

UC Office of the President

Recent Work

Title

Conceptual design of a high-sensitivity small animal PET camera with 4π coverage

Permalink

<https://escholarship.org/uc/item/55g2s0fs>

Authors

Huber, Jennifer S
Moses, William W.

Publication Date

1999

DOI

10.1109/23.775569

Peer reviewed

Conceptual Design of a High-Sensitivity Small Animal PET Camera with 4 Coverage*

J. S. Huber, *Member, IEEE* and W.W. Moses, *Senior Member, IEEE*
Lawrence Berkeley National Laboratory, University of California, Berkeley, CA 94720

Abstract

We present a conceptual design of a high-sensitivity PET camera that completely encloses a small animal in a rectangular volume formed by 6 planar banks of detector modules. The 4 geometry and 3 attenuation-length fast scintillators provide significantly higher sensitivity than contemporary animal PET cameras, while the depth of interaction (DOI) measurement and small crystal width achieve isotropic, high spatial resolution. The absolute sensitivity is 24 kcps/ μ Ci, \sim 120 times higher than contemporary systems; the true event count rate is increased by covering 10 times the solid angle using 80% efficient detectors. For a 29 g “mouse”, the total scatter event rate is 11% of the total true event rate. A short (2 nsec) coincidence window and the absence of out of field activity implicit with whole animal coverage yield a small random fraction. Assuming a maximum system count rate of 10 Mcps (achievable with electronics under development), the noise equivalent count rate as a function of activity concentration has a maximum of 6.6 Mcps at 25 μ Ci/cc. 2D reconstruction algorithms indicate a spatial resolution of 2.3 mm fwhm through most of the field of view.

I. INTRODUCTION

A number of high-resolution PET cameras optimized for small animal imaging have been developed [1-9]. Most are scaled-down versions of the conventional PET ring design, often with design trade-offs made to optimize spatial resolution. The ring diameter is small to minimize acollinearity effects, maximize sensitivity, and minimize cost. Compared to conventional PET cameras, “thinner” (*i.e.* less than 3 attenuation-lengths thick) detectors are often used to minimize radial elongation artifacts and worse energy resolution is often tolerated as the scatter backgrounds are less severe.

We propose a small animal PET camera that has both high sensitivity and high resolution. The animal is completely enclosed in a rectangular “patient” volume formed by 6 planar banks of PET detector modules (each bank 7.5 x 7.5 cm² or 7.5 x 10 cm²), providing 4 coverage as shown in figure 1(a). Each detector module [10] utilizes an array of 3 x 3 x 30 mm³ optically isolated LSO [11] scintillator crystals, coupled on one end to a photomultiplier tube (PMT) and on the opposite end to an array of 3 mm square silicon photodiodes (PD) as shown in figure 1(b). The PMT provides timing pulse and initial energy discrimination, the PD identifies the crystal of

interaction, the PD+PMT sum measures the total energy, and the PD/(PD+PMT) ratio measures the depth of interaction (DOI) along the crystal. Thus, this camera design has the advantage of both high sensitivity, from complete solid angle coverage and 3 attenuation-length fast scintillators, and good spatial resolution from small crystal width and DOI measurement. Other detector module designs — provided they have high efficiency, short dead time, and DOI measurement capability — could be used in this 4 geometry.

This camera design is a modification of a camera design optimized for breast imaging [12]. The PEM camera under development is made up of only 4 detector banks, shown in figure 1(a) in light gray. In this paper, we are investigating the use of two additional detector banks (shown in figure 1(a) in dark gray) to create a small animal PET camera.

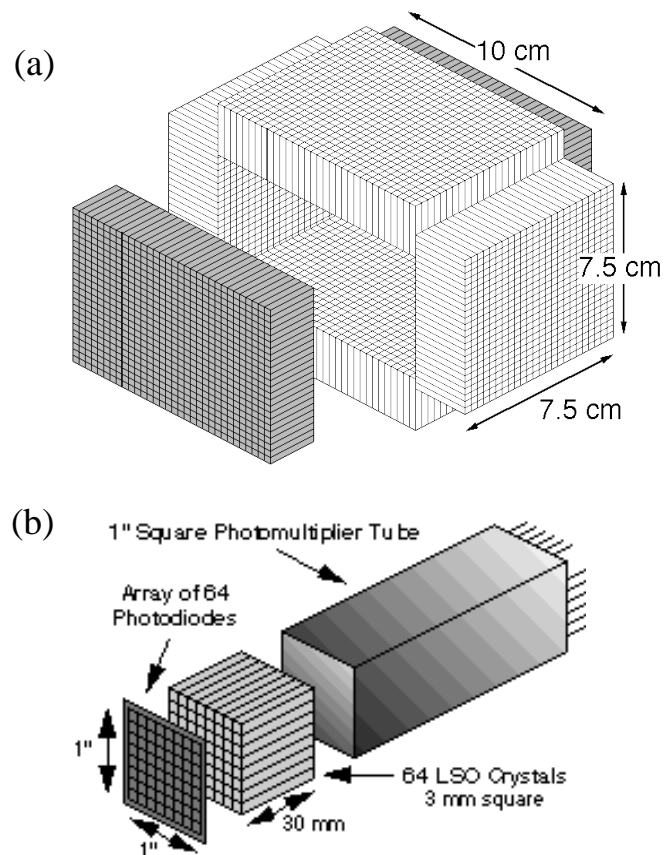


Figure 1: (a) Proposed LBNL camera design using 6 banks of detector modules to completely enclose a small animal. (b) Exploded view of the proposed PET module. Each LSO crystal is attached to a 1" square PMT (to provide timing pulse and energy discrimination) and to an individual photodiode (to identify the crystal of interaction). The PMT and PD signals are combined to measure the total energy ($E=PD+PMT$) and depth of interaction (PD/E).

* This work was supported in part by the U.S. Department of Energy under Contract No. DE-AC03-76SF00098, in part by Public Health Service Grant Nos. P01-HL25840 and R01-CA67911, and in part by Breast Cancer Research Program of the University of California Grant No. 1RB-0068.

II. METHODS

Analytic computation is used to estimate the sensitivity and count rate performance of cameras imaging water filled cylindrical phantoms with uniform activity concentration. The main assumption in this computation is that all detector modules are exposed to the same radiation flux, and so have the same singles rate, scatter fraction, coincidence fraction, and dead time factors. This computation includes the camera solid angle coverage and detection efficiency, effects of energy discrimination, coincidence timing window and random background, scatter and attenuation in the phantom, and dead time in the front-end and coincidence processing electronics.

Monte Carlo data are used to estimate the singles detection efficiency, scatter fraction, and coincidence detection efficiency. We obtain these factors by simulating simple cylindrical or spherical camera geometries with a water filled cylindrical phantom placed at the center of the camera. Energy dependent Compton scattering and photoelectric absorption are modeled in the phantom and detectors. Monte Carlo data are used to estimate the percentage of events that are within a photopeak window, using a 350 keV energy threshold. Detector scatter is thus incorporated in the Monte Carlo model by what fraction of the 511 keV photons fall within the photopeak window. The threshold choice of 350 keV was arbitrary and should be explored further using a real PET detector. The analytic computation does not explicitly perform scatter subtraction. Instead, the total scatter event rate is assumed to be a fixed fraction of the total true coincidence event rate; Monte Carlo simulation is used to determine the fraction. We are assuming an uniform scatter and random distribution (*i.e.* the same for every chord).

We first model using Monte Carlo data for a fixed activity strength, then analytically scale in order to determine the activity strength dependence. The true coincidence and scatter event rates are given by $True = \rho^2 \epsilon^2 g_t P^2$ and $Scatter = f_s True$ respectively, where ρ is the activity density, ϵ is the singles detection efficiency, g_t is a geometry efficiency for true coincidence events, P is the probability of escape for a 511 keV photon from the object, and f_s is the scatter fraction. The random event rate is given by $Random = 2\tau (Singles)^2 = 2\tau \rho^2 \epsilon^2 g_r P^2$ where τ is the coincidence resolving time and g_r is a geometry efficiency for random events. These rates are modified to reflect detector dead time and coincidence processor rate limitations, and the proportionality factors are determined either from first principles or by comparing to published data. The dead time effects are imposed using two factors — a paralyzing dead time efficiency per module due to the front-end electronics, modeled as an exponential, and a maximum system event rate limit due to the coincidence processing electronics. When the total system event rate exceeds the maximum, the individual count rates (*i.e.* true coincidence, random and scatter count rates) are taken as relative fractions of the maximum.

The noise equivalent count rate (NECR) is the number of counts detected as a function of the activity concentration, after

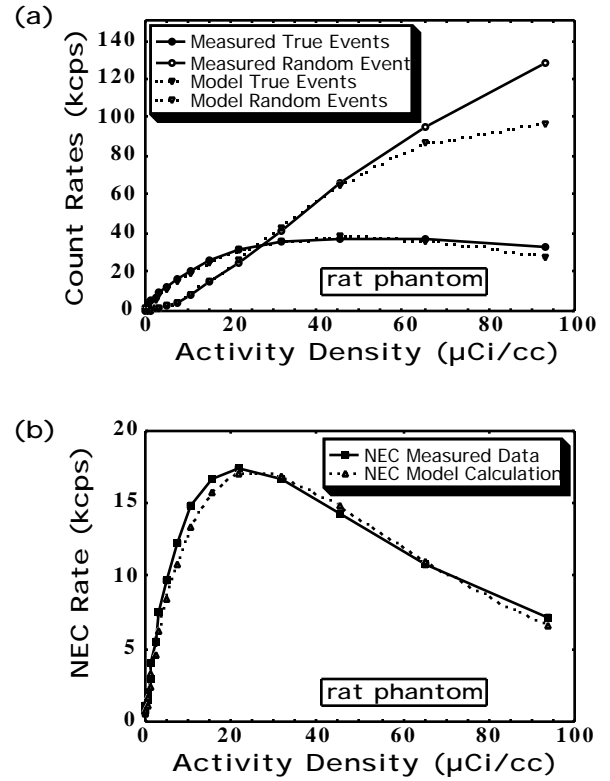


Figure 2: Comparison between measured (solid lines) and modeled (dashed lines) count rates of the MicroPET system for a 2.5" diameter by 1.5" long cylindrical "rat" phantom of uniform activity. (a) True coincidence and random event rates and (b) noise equivalent count rates as a function of phantom activity concentration. Calculated and measured curves agree within 13% on average, demonstrating good modeling accuracy.

correcting for the effects of random and scatter events and taking into account dead time losses. It is a standard measure of signal to noise in reconstructed PET images [13]. When calculating the NECR, only random and scatter events in the field of view of the object contribute.

We validate this analytic-computation model using measured data from MicroPET [5], an existing small animal PET camera whose performance is well characterized. MicroPET is basically a scaled down version of a conventional PET camera designed for imaging a variety of animals, including primates, rats, and mice. It consists of a ring of 30 position-sensitive scintillation detectors, each with an 8 x 8 array of 2 x 2 x 10 mm³ LSO crystals coupled via optical fibers to a multi-channel photomultiplier tube. The detector ring diameter is 17.2 cm with an axial extent of 1.8 cm.

We compare between our MicroPET model and measured data when imaging a small "rat" phantom placed at the camera center. This 120 cc water filled cylindrical phantom, with a 2.5" diameter and 1.5" length, is the smallest phantom for which MicroPET has data available. Figure 2 shows the true coincidence event, random event, and noise equivalent count rates as a function of activity concentration of the MicroPET system for both measured and our modeled data. Calculated and measured curves agree within 4% for the majority of the

activity density range and within 13% on average, demonstrating good modeling accuracy. Some disagreement is seen for random and true coincidence event rates at the highest activity density; we believe this is due to the simplicity of our dead time model.

III. LBNL ANIMAL PET CAMERA DESIGN

A. Count Rates and Sensitivity

The analytic computation is then used to estimate the performance of our LBNL small animal PET camera, compared with calculated MicroPET performance. We apply the model to a “mouse” phantom — a 29 cc water filled cylinder with a 2.5 cm diameter and 6 cm length — placed at the center of either camera.

We model the LBNL camera design assuming a 10 Mcps maximum system count rate, which is limited by the coincidence processing electronics. Figure 3 shows the true coincidence, scatter, random, and total event rates as a function of phantom activity concentration calculated with this camera design when imaging the “mouse” phantom. We predict a very large true coincidence event rate, which dominates the total event rate for the entire range of activity concentrations shown. Our random fraction is small due to a short (2 nsec) coincidence window and the absence of “out of field” activity implicit with whole animal coverage. The total scatter event rate is assumed to be 11% of the total true coincidence event rate, based on Monte Carlo simulation.

The noise equivalent count rate as a function of activity density for the LBNL camera with the “mouse” phantom is shown in figure 4. The maximum NECR is 6600 kcps at an activity concentration of 25 $\mu\text{Ci/cc}$, limited by the data acquisition system. If the maximum system count rate is removed, the LBNL camera maximum NECR becomes 8100 kcps at 45 $\mu\text{Ci/cc}$ and is limited by the front-end electronics. We compare our results with the calculated NECR for the

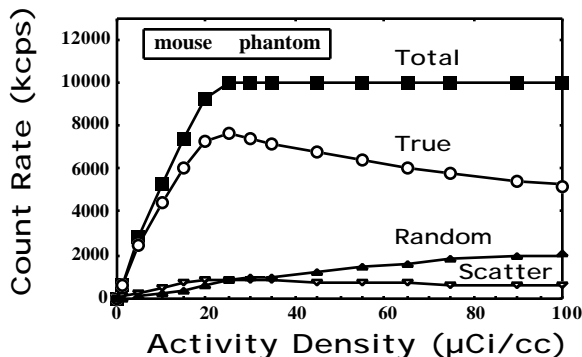


Figure 3: True coincidence, scatter, random and total event rates as a function of phantom activity concentration calculated for the proposed LBNL animal PET camera with a 29 cc “mouse” phantom. The random fraction is small due to the absence of “out of field” activity implicit with complete solid angle coverage, as well as a short coincidence window. The total scatter event rate is 11% of the total true event rate. A maximum system count rate of 10 Mcps is assumed.

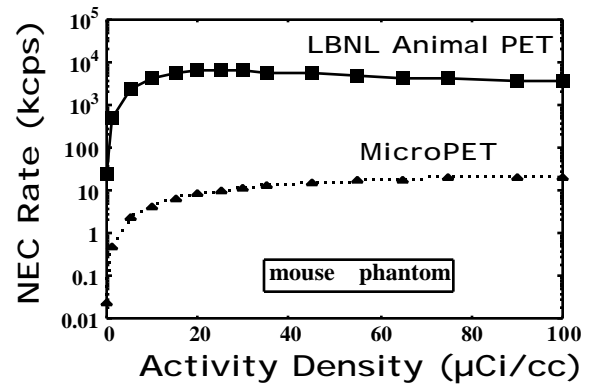


Figure 4: Noise equivalent count rate as a function of phantom activity concentration calculated for the proposed LBNL camera design (solid line) and MicroPET (dashed line) with a 29 cc “mouse” phantom.

MicroPET system when imaging the same “mouse” phantom, also shown in figure 4 as a function of activity density. MicroPET has a maximum NECR of 22 kcps at a concentration of 100 $\mu\text{Ci/cc}$. Thus, we predict much higher noise equivalent count rates for the LBNL camera.

The absolute sensitivity is calculated for a point source at the center. The absolute sensitivity of the LBNL camera is 24 kcps/ μCi , approximately 120 times higher than the measured MicroPET system sensitivity. The increase is due to covering more solid angle (factor of 10) and using detector modules with 80% photopeak efficiency rather than ~23% efficiency (factor of 12). The large increase in sensitivity, while maintaining good spatial resolution, should provide a significantly improved small animal PET camera for many applications.

B. Data Acquisition

With complete solid angle coverage and an assumed maximum system event rate of 10 Mcps, the LBNL camera count rate is very large. In addition, a 38 bit coincidence event word will be needed. However, new architectures for higher performance data acquisition in PET are currently under development [14]. These proposed new architectures are expected to include a 64 bit coincidence event word, on-line rebinning for DOI, and a throughput of 10 M events/sec for list-mode data collection as well as both on-line and replay histogramming. The simplest data acquisition scheme is to collect data in list-mode, which would fill a 47 Gbyte disk in 10 minutes at the maximum event rate.

Histogramming based data collection is also possible. If we have 8 depths per crystal, approximately 474 M lines of response are expected. This implies that we will have 3.8 Gbytes of data. After rebinning, we expect 7.4 M chords; this is estimated using combinatorics with the assumption of connecting only the front face of each crystal. The actual binning will be discussed further in the next section. This corresponds to 59 Mbytes of data. Thus, data collection at the assumed maximum rate of 10 Mcps is possible using electronics presently under development.

C. Reconstruction

The LBNL rectangular PET camera design requires us to address some reconstruction issues: we must handle uneven sampling; we are allowing the object to fill the camera; and we must determine how best to use the depth of interaction data. However, these issues have been solved in two dimensions [15] using a two-dimensional filtered back-projection algorithm with even radial binning and irregular angular sampling. We reconstruct artifact free images with a nearly isotropic and position independent spatial resolution of 2.3 mm full width at half maximum (fwhm). Some degradation (up to 2.8 mm fwhm) is observed in the corners of the detector where penetration effects are the worst, but it is unlikely that the animal would be located in these positions.

We are currently investigating how to extend this algorithm to three dimensions. The primary task is to determine how best to parameterize the data, taking advantage of the increased sampling gained with the depth of interaction information. After rebinning, fully three-dimensional reconstruction algorithms will be applied to the data. This reconstruction will be simplified since there will be no truncated data due to our 4π coverage. For instance, we could directly apply Colsher's fully three-dimensional PET algorithm [16].

In order to correct for attenuation, we plan to use an immobilizing holder and CAT scan the animal. We can also calculate the attenuation correction factors with moderate errors since the corrections will be relatively small; the typical correction factor is $\sim 30\%$ for a mouse. Scatter subtraction will be easier to implement than in conventional cameras, since all activity sources and scatterers will be within the FOV for our camera with full solid angle coverage. The scatter fraction is also small — $\sim 10\%$ for a mouse. Normalization will be done using a Plexiglas box of uniform activity. There are issues concerning detector calibration, but we have previously reported on two “*in situ*” calibration techniques [17].

IV. DISCUSSION

We expect this camera to be primarily used in the development and characterization of new pharmaceuticals or to study gene expression *in vivo* [18]. Due to the noninvasive characteristics of PET, it would allow us to perform repeated scans of the same animal to reduce inter subject variability. The camera could also be used to measure the effectiveness and action of new forms of therapy in cancer and possibly neurological disease, allowing progress to be tracked in the same animal.

Fine spatial resolution is desired when imaging small animals in order to minimize partial volume errors. Our predicted reconstruction resolution of 2.3 mm fwhm could be improved with the use of finer LSO crystals, although the increased electronics density provides challenges.

One might question whether the proposed camera is “too sensitive” and provides more counts per unit injected activity than is necessary. However, the sensitivity required for studies

in laboratory animals is a complicated issue, particularly for kinetic studies. For instance, Hume *et al.* point out that the injected radioactivity is often limited by the specific activity especially when using high affinity ligands [19,20]. For this case, and when performing studies with fine temporal resolution, high sensitivity is mandatory. While the level of activity concentration that is realistic will depend on the compound and experiment, the increased sensitivity of our proposed camera design should allow studies to be run successfully at relatively low activity concentrations.

This camera design would probably require the addition of gaps for anesthesia and air supply lines. However, this should only have a minor impact on the 4π geometry. A more versatile design could be made by eliminating the 7.5×7.5 cm² detector banks on either end. This would provide increased access to the animal, while still maintaining approximately 77% of the 4π solid angle coverage using 80% efficient detectors.

V. CONCLUSIONS

This paper has described a conceptual design of a high-sensitivity small animal PET camera with full solid angle coverage. When imaging a mouse phantom, we predict a high sensitivity of 24 kcps/ μ Ci and high peak NECR of 6.6 Mcps at 25 μ Ci/cc. We demonstrate good spatial resolution with a 2.3 mm fwhm reconstruction resolution through most of the FOV. Three-dimensional reconstruction is expected to be made easier by 4π detection and the depth of interaction information. Data collection, even at the maximum rate of 10 Mcps, is possible with electronics currently under development. Hence, we have demonstrated the potential for a significantly improved small animal PET camera.

VI. ACKNOWLEDGMENTS

We wish to thank Dr. Simon Cherry for providing us with MicroPET count rate and sensitivity data, thus allowing us to make these comparisons. We would also like to thank Patrick Virador for his assistance with the Monte Carlo simulation and Ron Huesman for his shared expertise in data reconstruction. And we would like to thank CTI PET Systems, especially John Young, Bill Jones, John Reed, Cliff Moyer, Chuck Melcher, Mark Andreaco, and Ron Nutt, for their useful conversations concerning detector and electronics development. This work was supported in part by the Director, Office of Energy Research, Office of Biological and Environmental Research, Medical Applications and Biophysical Research Division of the U.S. Department of Energy under contract No. DE-AC03-76SF00098, in part by the National Institutes of Health, National Heart, Lung, and Blood Institute, and National Cancer Institute under grants No. P01-HL25840 and R01-CA67911, and in part by the Breast Cancer Fund of the State of California through the Breast Cancer Research Program of the University of California under grant No. 1RB-0068.

VII. REFERENCES

- [1] P.M. Bloomfield, S. Rajeswaran, et al., "The design and physical characteristics of a small animal positron emission tomograph," *Phys. Med. Biol.*, vol. 40, pp. 1105, 1995.
- [2] X. Liu, S. Rajeswaran, et al., "Design and physical characteristics of a small animal PET using BaF₂ crystals and a photo sensitive wire chamber," *Nucl. Instrum. and Meth. A*, vol. 382, pp. 589, 1996.
- [3] R. Lecomte, J. Cadorette, et al., "Initial results from the Sherbrooke avalanche photodiode positron tomograph," *IEEE Trans. Nucl. Sci.*, vol. NS-43, pp. 1952, 1996.
- [4] A. Del Guerra, F. de Notaristefani, et al., "Use of a YAP:Ce matrix coupled to a position-sensitive photomultiplier for high resolution positron emission tomography," *IEEE Trans. Nucl. Sci.*, vol. NS-43, pp. 1958, 1996.
- [5] S.R. Cherry, Y. Shao, et al., "MicroPET: A High Resolution PET Scanner for Imaging Small Animals," *IEEE Trans. Nucl. Sci.*, vol. NS-44, pp. 1161, 1997.
- [6] M. Watanabe, H. Okada, et al., "A High Resolution Animal PET Scanner Using Compact PS-PMT Detectors," *IEEE Trans. Nucl. Sci.*, vol. NS-44, pp. 1277, 1997.
- [7] O. Fries, S.M. Bradbury, et al., "A small animal PET prototype based on LSO crystals read out by avalanche photodiodes," *Nucl. Instrum. and Meth. A*, vol. 387, pp. 220, 1997.
- [8] S. Weber, A. Terstegge, et al., "The Design of an Animal PET: Flexible Geometry for Achieving Optimal Spatial Resolution or High Sensitivity," *IEEE Trans. Med. Imaging.*, vol. 16, pp. 684, 1997.
- [9] A.P. Jeavons, R.A. Chandler, et al., "A Fully-3D, Low Cost PET Camera using HIDAC Detectors with Sub-millimeter Resolution for Imaging Small Animals," *submitted to IEEE Trans. Nucl. Sci.*, 1998 .
- [10] J.S. Huber, W.W. Moses, et al., "Characterization of a 64 Channel PET Detector Using Photodiodes for Crystal Identification," *IEEE Trans. Nucl. Sci.*, vol. NS-44, pp. 1197, 1997.
- [11] C.L. Melcher and J.S. Schweitzer, "Cerium-doped lutetium orthosilicate: A fast, efficient new scintillator," *IEEE Trans. Nucl. Sci.*, vol. NS-39, pp. 502, 1992.
- [12] W.W. Moses, T.F. Budinger, et al., "PET camera designs for imaging breast cancer and axillary node involvement," *J. Nucl. Med* 36: pp. 69P, 1995.
- [13] S.C. Strother, M.E. Casey, et al., "Measuring PET Scanner Sensitivity: Relating Count Rates to Image Signal-to-Noise Ratios using Noise Equivalent Counts," *IEEE Trans. Nucl. Sci.*, vol. NS-37, pp. 783, 1990.
- [14] W.F. Jones, J.H. Reed, et al., "Next Generation PET Data Acquisition Architectures," *IEEE Trans. Nucl. Sci.*, vol. NS-44, pp. 1202, 1997.
- [15] P.R.G. Virador, W.W. Moses, et al., "Reconstruction in PET Cameras with Irregular Sampling and Depth of Interaction Capability," *IEEE Trans. Nucl. Sci.*, vol. NS-45, pp. 1225, 1998.
- [16] J.G. Colsher, "Fully three-dimensional positron emission tomography," *Phys. Med. Biol.*, vol. 25, pp. 103, 1980.
- [17] J.S. Huber, W.W. Moses, et al., "Calibration of a PET Detector Module that Measures Depth of Interaction," *IEEE Trans. Nucl. Sci.*, vol. NS-45, pp. 1268, 1998.
- [18] Society of Nuclear Imaging in Drug Development, "Symposium on the Use of Imaging in Drug R&D," Bethesda, MD, Sept. 11-13, 1998. Conference Proceedings *J. Clin. Pharm.*, in press.
- [19] S.P. Hume and T. Jones, "Pharmacological constraints associated with positron emission tomographic scanning of small laboratory animals," *Eur J Nucl Med*, vol. 25, pp. 173, 1998.
- [20] S.P. Hume and T. Jones, "Positron Emission Tomography (PET) Methodology for Small Animals and Its Application in Radiopharmaceutical Preclinical Investigation," *Nucl Med Biol*, vol. 25, pp. 729, 1998.